Doctoral Dissertation (Censored)

博士論文（要約）

A Generalized Mechanism of the Primary Photoreaction in Microbial Rhodopsins as Revealed by Femtosecond Time-Resolved Spectroscopy

（フェムト秒時間分解分光による微生物型ロドプシンの光反応初期過程の機構解明）

A Dissertation Submitted for the Degree of Doctor of Science

December 2019

令和元年１２月博士（理学）申請

Department of Chemistry, Graduate School of Science,

The University of Tokyo

東京大学理学系研究科化学専攻

Chun-Fu Chang

張　君輔

Abstract

Despite the diverse biological functions in different microbial rhodopsins, all these functions are triggered by the same primary photoreaction, i.e., all-*trans* to *13-cis* photoisomerization of the protonated retinal Schiff base (PRSB) chromophore, which occurs on the femto-to-picosecond time scale. Therefore, elucidation of the mechanism of the photoisomerization in microbial rhodopsins enriches our fundamental knowledge about how light energy is converted into chemical potential in nature. While the mechanism of the photoisomerization has been extensively studied, one of the issues still under debate is the origin of multi-exponential decays of the excited-state population including the fast (<1 ps) and slow (>1 ps) decay components, which are observed in many rhodopsins. In order to obtain a generalized picture of the primary photoisomerization process in microbial rhodopsins, several prototypical microbial rhodopsins were thoroughly investigated by femtosecond time-resolved spectroscopy in this thesis study.

The author studied the primary photoreaction dynamics of the proton (H^+)-pumping rhodopsins, i.e., proteorhodopsin (PR), its D97N mutant and bacteriorhodopsin (BR), which were investigated in a wide pH range by femtosecond time-resolved absorption spectroscopy. Quantitative analysis of the time-resolved absorption spectra confirmed that the excited state decays multi-exponentially, containing the fast (<1 ps) and slow (>1 ps) decay components. More importantly, the excited-state relaxation dynamics and the retinal photoisomerization efficiency were strongly correlated with the protonation state of the corresponding PRSB counterion (Asp97 for PR and Asp85 for BR, respectively): When the PRSB counterion is deprotonated, the excited state predominantly decays with the fast (<1 ps) decay component and proceeds efficient photoisomerization. Such a

correlation indicates that the equilibrium of the protonated/deprotonated PRSB counterion in the ground state is the molecular origin of the multi-exponential decay of the excite state. This conclusion was further supported by the study on the photoisomerization dynamics of the recently discovered TAT rhodopsin. In TAT rhodopsin, the analogue position of the PRSB counterion is neutral Thr82, which is considered equivalent to that of PR and BR when the counterion is protonated. As expected, the retinal photoisomerization was extremely inefficient and the excited-state population decayed exclusively with the slow (>1 ps) decay components. Furthermore, the impulsive stimulated Raman measurements of PR found that the retinal chromophore is distorted when the PRSB counterion Asp97 is protonated. The author suspects that the distorted chromophore structure may not be optimized for efficient retinal isomerization, giving rise to a lower photoisomerization reactivity when the counterion Asp97 is protonated.

In conclusion, the protonation state of the PRSB counterion plays a decisive role in determining the excited-state dynamics and the photoisomerization reactivity of microbial rhodopsins in general. Although the complex excited-state relaxation dynamics in different rhodopsins have been explained with difference in the branching of the relaxation pathway on the S_1 PES, the present study unambiguously showed that the difference, in fact, originates from the difference in the structure in the ground state of microbial rhodopsin, i.e., difference in the protonation state of the PRSB counterion. The present study provides a new, coherent view about the primary photoreaction in retinal proteins.

Table of Contents

Chapter 1.

General Introduction

1.1 Microbial Rhodopsins

Rhodopsins are photoreceptor proteins which are ubiquitous in all life domains. They can be classified into two groups, i.e., microbial (type-1) rhodopsins and animal (type-2) rhodopsins.[1,2] Both microbial and animal rhodopsins share a common protein structure consisting of seven transmembrane α-helices that are aligned across the cell membrane, and a retinal molecule is linked covalently with helix G through the protonated Schiff base linkage of the lysine residue, namely the protonated retinal Schiff base (PRSB) chromophore (Figure 1.1). Animal rhodopsins are the representatives of G-protein coupled receptors,[3] which contain the PRSB chromophore in *11-cis* conformation and serve as visual pigments. Microbial rhodopsins, on the other hand, are found in microorganisms in Archaea and bacteria, having the PRSB chromophore in all-*trans* conformation.

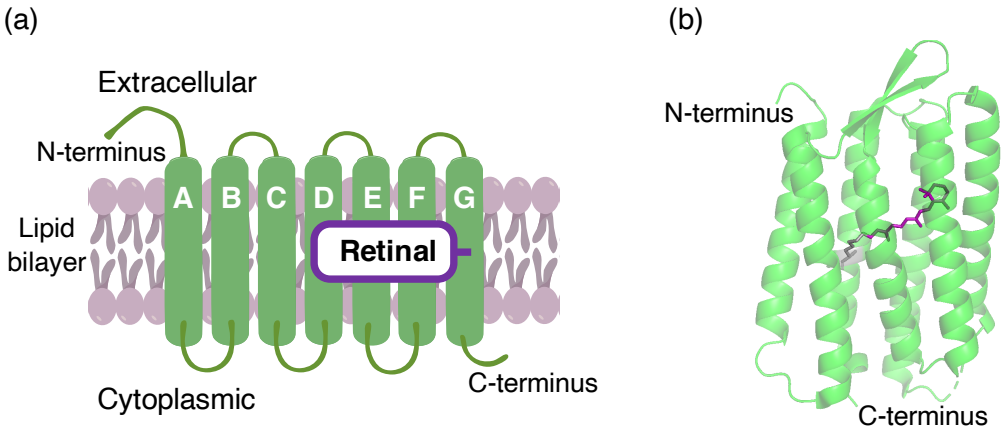

Figure 1.1 Structure of microbial rhodopsin. (a) Seven α-helical transmembrane (denoted in helix A–G) aligned across the lipid bilayer. The retinal chromophore is bound covalently to the helix G. The N-terminus faces outside of the cell, and the C-terminus is inside of the cell. (b) Three-dimensional view of the seven transmembrane (green) with the attached all-*trans* PRSB chromophore (purple) in a microbial rhodopsin (bacteriorhodopsin, PDB ID: 1C3W).

Unlike monofunctional animal rhodopsins, microbial rhodopsins have various biological functions, such as light-driven ion pump, light-gated ion channel, and light sensors (Figure 1.2).[2,4] Because of the ion-transporting capability, microbial rhodopsins have become a tool in optogenetics, recently.[5] The relevant biological function is driven by absorption of a photon, which initiates all-*trans* to *13-cis* photoisomerization of the retinal chromophore. The chromophore isomerization subsequently triggers a series of protein structural change to complete a cyclic reaction (photocycle) and realizes its biological function.

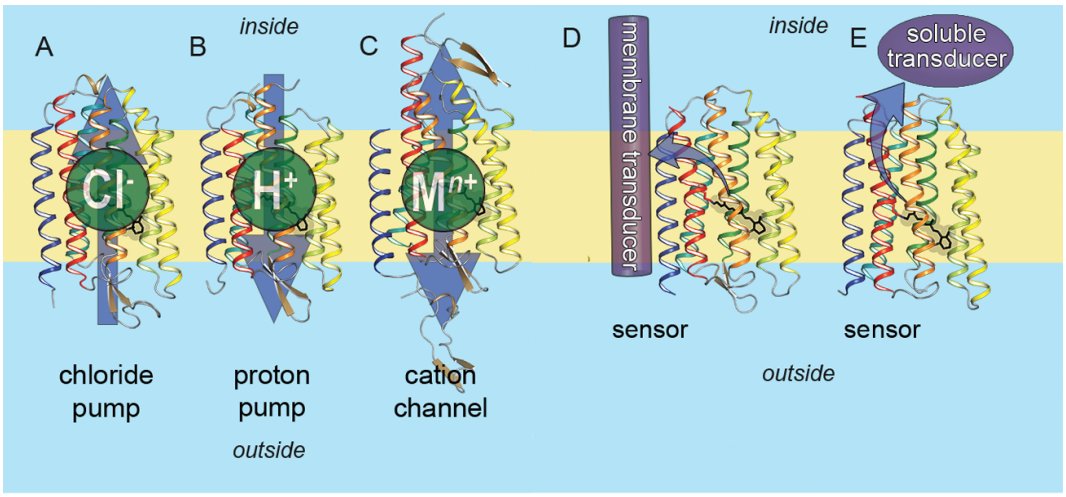

Figure 1.2 Various biological functions of different microbial rhodopsins. Arrows indicate the direction of ion transport or signal flow. (a) light-driven inward chloride pump (halorhodopsin, PDB ID: 1E12), (b) light-driven outward proton pump (bacteriorhodopsin, PDB ID: 1C3W), (c) light-gated ion channel (channelrhodopsin, PDB ID: 3UG9), (d) light-sensor activating membrane transducer protein (sensory rhodopsin II, PDB ID: 1JGJ), (e) light-sensor activating soluble transducer protein (*Anabaena* sensory rhodopsin, PDB ID: 1XIO). Reproduced with permission from *Chem. Rev.* 2014, 114, 126. Copyright (2013) American Chemical Society.

Bacteriorhodopsin (BR) is the first discovered microbial rhodopsin in 1971 from the cell membrane of the halophilic bacterium *Halobacterium halobium*, and it functions as a light-driven outward proton (H^+) pump.[6] BR is the most well-studied rhodopsin, and it is considered as the paradigm of a light-driven ion-pumping rhodopsin and a template for understanding other rhodopsins discovered later.[7-9]

Here, the photocycle of BR is briefly reviewed as an example for explaining how the rhodopsin functions in the microorganism. Figure 1.3(a) shows the photocycle of BR for transporting the H^+ across the membrane from cytoplasmic to extracellular side.[2] Upon light illumination, all-*trans* PRSB chromophore undergoes ultrafast photoisomerization and yields the hot ground-state intermediate J, which relaxes to the K intermediate that contains twisted *13-cis* retinal chromophore on a picosecond time scale. Such isomerization of the retinal chromophore stores sufficiently high free energy (40–50 kJ/mol) upon thermal relaxation, to induce subsequent change of the protein structure.[10,11] Relaxation of the structural strain in the chromophore in K leads to the L intermediate. This L intermediate is the precursor that sets up the stage for the following H^+ transfer reactions. Figure 1.3(b) shows the vectorial H^+ transfer pathway across the cell membrane from cytoplasmic to extracellular side. The first H^+ transfer occurs from the protonated Schiff base to its primary H^+ acceptor Asp85 (step ① in Figure 1.3(b)), giving rise to formation of the M intermediate. Simultaneously, a H^+ is released to the extracellular side (step ② in Figure 1.3(b)) through a paired H^+ release complex Glu194-Glu204. In the N intermediate state, the Schiff base is reprotonated by its primary H^+ donor Asp96 (step ③ in Figure 1.3(b)). Asp96 subsequently regains a H^+ from the cytoplasmic side (step ④ in Figure 1.3(b)), which is followed by thermal relaxation of the retinal from the *13-cis* to all-*trans* conformation, yielding the O intermediate. Finally, Asp85 deprotonates and the H^+ is transferred to the H^+ release complex Glu194-Glu204

(step ⑤ in Figure 1.3(b)), and BR returns to the original ground state to complete the photocycle. Transportation of H^+ across the cell membrane of BR creates the pH gradient, which is used for synthesizing adenosine triphosphate (ATP) in the Halobacterium.

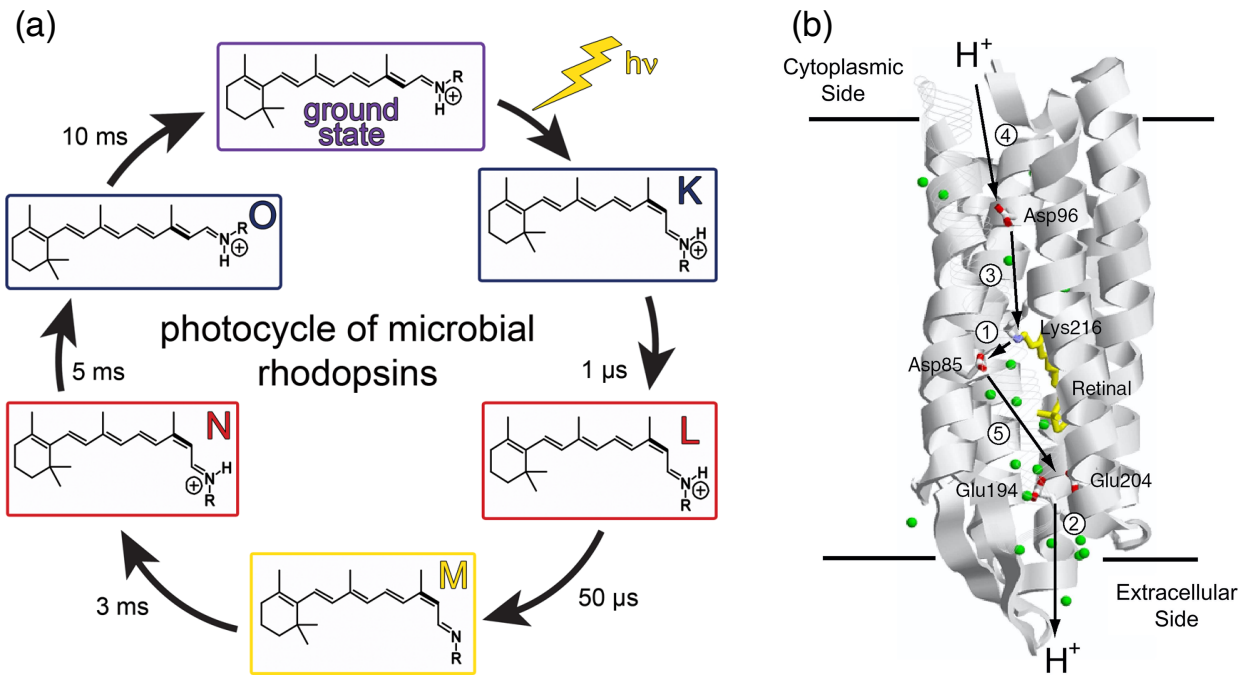

Figure 1.3 (a) Photocycle of BR with the isomeric and protonation states of the PRSB chromophore in each intermediate.[2] The time constants indicate the lifetime of each intermediate state. Reprinted with permission from *Chem. Rev.* 2014, 114, 126. Copyright (2013) American Chemical Society. (b) Vectorial H^+ transport pathway during the photocycle of BR (PDB ID: 1C3W).[4] The amino acid residues and internal water molecules (green spheres) important for H^+ transport are shown. The arrows indicate the direction of H^+ transport. Reprinted with permission from *Front. Mol. Biosci.* 2015, *2*, 52. Copyright (2015) Kandori.

1.2 Primary Photoreaction in Microbial Rhodopsins

Despite the diverse functionalities of microbial rhodopsins, all these functions are initiated by the same primary photoreaction, i.e., all-*trans* to *13-cis* photoisomerization of the PRSB chromophore, which occurs on a femto-to-picosecond time scale (Figure 1.4). The primary photoisomerization is very efficient in microbial rhodopsins that eventually realize their biological functions. In fact, the quantum yield of the photoisomerization in microbial rhodopsins can be as high as 0.3–0.7, and the photoproduct is highly specified to the *13-cis* retinal isomer.[12-14] This is in sharp contrast to the low quantum yield (~0.1) and lack of isomeric selectivity of the photoproduct in the photoisomerization of free PRSB molecules in methanol solution.[15,16] This implies that the interaction between the PRSB chromophore and the protein binding pocket plays a decisive role in the primary photoisomerization reaction. Therefore, elucidation of the mechanism of the primary photoisomerization in microbial rhodopsins deepens our fundamental knowledge of photochemical reactions in nature.

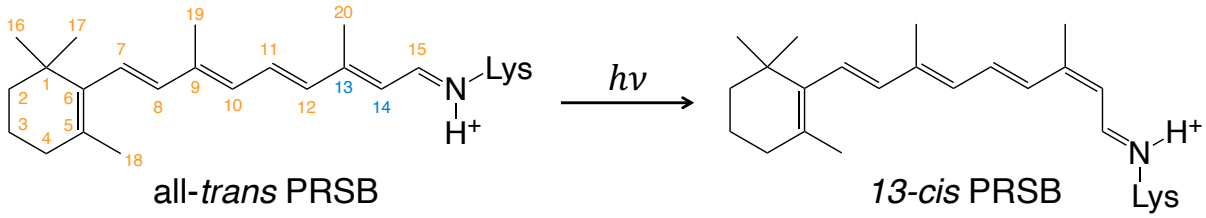

Figure 1.4 Schematic of primary photoisomerization of the all-*trans* PRSB chromophore in microbial rhodopsin. The numbering of the carbon atoms is also shown.

The ultrafast dynamics of primary photoreaction in different microbial rhodopsins have been extensively studied.[17-22] As in the case of the most well-known rhodopsin BR, it has been reported that the primary photoisomerization of the all-*trans* PRSB proceeds with single exponential decay

of the excited-state population with a 0.5-ps time constant along with formation of the *13-cis* form (the J intermediate).[17,23,24] However, other microbial rhodopsins exhibit much more complicated decays of the excited-state population during the primary photoisomerization process. For example, halorhodopsin[18,19], proteorhodopsin (PR)[20,25] and *Anabaena* sensory rhodopsin[21,26] exhibit biexponential decay of the excited state, while KR2 shows tri-exponential decay.[22] To rationalize the multi-exponential decay of the excited state of these rhodopsins, the branching model depicted in Figure 1.5(a) has been used for a long time.[18-20,27,28] In this model, the multi-exponential decay is attributed to the branching of the relaxation pathways into different minima of the S_1 potential energy surface (PES), from which the excited-state relaxation proceeds with different rates. Usually, it was considered that the fast (<1 ps) decay pathway preferentially yields the photoproduct, whereas the slow (>1 ps) decay pathway predominantly relaxes back to the original ground state.

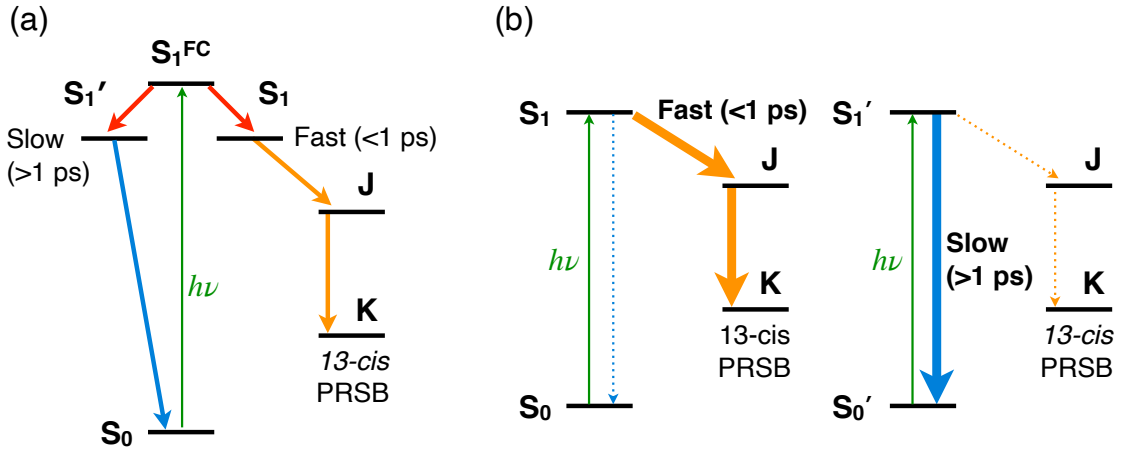

Figure 1.5 Schematic of the reaction models for the primary photoreaction in microbial rhodopsin: (a) the branching model, (b) the heterogeneity model. S_1^{FC} denotes the S_1 Franck-Condon state while J and K are the photocycle intermediates in the S_0 state having *13-cis* retinal conformation. The solid lines indicate the major reaction pathways.

Very recently, the Tahara group studied the primary photoreaction of the sodium (Na^+)-pumping rhodopsin KR2 using femtosecond time-resolved absorption spectroscopy and found that its excited-state dynamics exhibits a multi-exponential decay, involving a sub-picosecond fast decay component and long-lived (>1 ps) slow decay components.[29] Furthermore, it was found that the relative amplitude of the sub-picosecond component is strongly dependent on pH and is well correlated with the acid/base equilibrium of the Asp116 residue, which is the counterion of the PRSB chromophore in KR2. In fact, the excited-state relaxation of KR2 sharply changes at around pH 7, which is in good accordance with the titration curve of Asp116. As such a correlation is not expected for the branching model, they concluded that the multi-exponential decay in KR2 arises from the acid–base equilibrium of the counterion Asp116 in the ground state. In other words, KR2 has both protonated or deprotonated Asp116 under physiological conditions, and these species are simultaneously photoexcited and exhibit different relaxation dynamics. These parallel excited-state relaxation processes were considered the origin of the multi-exponential decays observed in the femtosecond time-resolved absorption data. This model is called the heterogeneity model, and it is schematically illustrated in Figure 1.5(b). As sketched in this figure, in the heterogeneity model, the pH-dependence of the excited-state relaxation dynamics is explained in terms of the change of the relative population in the ground state having different structures (S_0 and S_0'), i.e., deprotonated and protonated PRSB counterions. On the other hand, in the branching model, the pH-dependence is rationalized as the change in the branching ratio required to generate the fast (<1 ps) S_1 and slow (>1 ps) S_1' decay pathways on the S_1 PES.

The pH-dependent ultrafast dynamics of KR2 strongly indicates that the origin of the multi-exponential decay of the excited state arises from the heterogeneity (the acid-base equilibrium of the counterion amino acid residue) in the ground state. However, KR2 is a special microbial

rhodopsin that has a peculiar Na^+-transporting function, which was thought to be prohibited by the electrostatic repulsion with the Schiff base proton before the discovery of KR2.[30] The recent X-ray crystallography study has revealed that the Na^+ is able to be transported in KR2 due to the unique chromophore environment, which is different from the environment in BR that has the ordinary H^+-pumping function (see Figure 1.6).[31] Specifically, the position of the PRSB counterion Asp116, which is the primary H^+ acceptor in the M intermediate, is different from that of counterion Asp85 in BR. The unusual position of the counterion Asp116 makes the Schiff base rotate differently and form unique hydrogen-bonding networks. This unique chromophore environment in KR2 questions the generality of the heterogeneity model proposed by the Tahara group:[29] It would be possible that the ground-state heterogeneity observed in KR2 is only because of its unique structure. Therefore, the generality of the heterogeneity model needs to be examined for rhodopsins that have the ordinary H^+-pumping function.

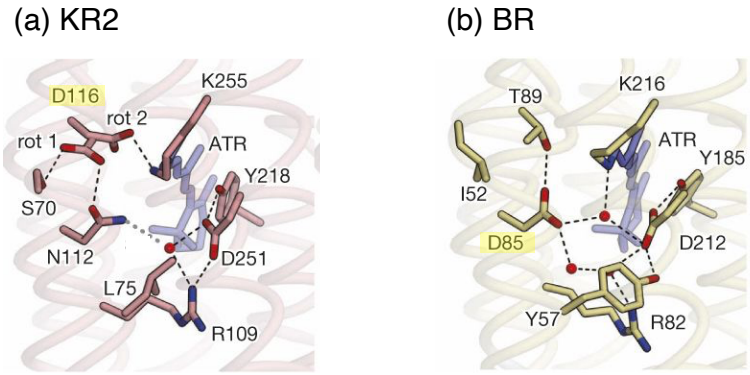

Figure 1.6 X-ray crystal structure of (a) KR2 and (b) BR in the Schiff base region at neutral pH.[31] ATR: all-*trans* retinal chromophore. The residues highlighted in yellow are the principal PRSB counterions (Asp116 for KR2 and Asp85 for BR, respectively). The red spheres and black dashed lines represent the internal water molecules and hydrogen bonds, respectively. Reprinted with permission from *Nature* 2015, 521, 48. Copyright (2015) Springer Nature.

1.3 Purpose and Contents of This Thesis Study

In this thesis study, the author is dedicated to obtaining a generalized and coherent picture of the primary photoreaction in microbial rhodopsins. The current models depicted in Figure 1.5 have the following questions: (1) In the branching model, it is unclear why the dynamics of different rhodopsins branches differently on their S_1 PESs, and the molecular origin of such branching is not yet understood. (2) In the heterogeneity model proposed for the Na^+-pumping rhodopsin KR2, it is still not clear whether it can be generally applied to other rhodopsins because it has been proposed for KR2 that has a unique chromophore environment. With the aim of answering these questions and providing a unified view of the primary process in microbial rhodopsins, the author utilized different femtosecond spectroscopic techniques and investigated the femtosecond-picosecond dynamics of the primary photoreaction of several prototypical microbial rhodopsins at systematically varied pH values.

The remainder of this thesis is organized as follows: In Chapter 2, the principles and experimental setups of the femtosecond spectroscopic techniques used in the present study are describe. In Chapter 3, femtosecond time-resolved absorption spectroscopic studies on the ultrafast dynamics and its pH dependence of the primary photoreaction in PR, its D97N mutant and BR having ordinary H^+-pumping function are discussed. It is shown that their excited-state relaxation dynamics strongly correlates with the protonation state of the PRSB counterion in the ground state. Based on these results, the generalized scheme of the primary photoreaction in rhodopsins is proposed. In Chapter 4, this generalized photoreaction scheme is applied to interpret femtosecond time-resolved absorption data of the recently discovered TAT rhodopsin. In Chapter 5, impulsive stimulated Raman spectroscopy of PR is discussed, which was performed to clarify the structural change of the retinal chromophore induced by the change of its counterion protonation state. At

last, in Chapter 6, the summary of the generalized primary photoreaction scheme that was clarified with this thesis study as well as the prospective experiments to solve the unanswered questions are described.

References

(1) Spudich, J. L.; Yang, C. S.; Jung, K. H.; Spudich, E. N. Retinylidene Proteins: Structures and Functions from Archaea to Humans. *Annu. Rev. Cell Dev. Biol.* **2000**, *16* (1), 365–392.

(2) Ernst, O. P.; Lodowski, D. T.; Elstner, M.; Hegemann, P.; Brown, L. S.; Kandori, H. Microbial and Animal Rhodopsins: Structures, Functions, and Molecular Mechanisms. *Chem. Rev.* **2014**, *114* (1), 126–163.

(3) Palczewski, K. G Protein-Coupled Receptor Rhodopsin. *Annu. Rev. Biochem.* **2006**, *75* (1), 743–767.

(4) Kandori, H. Ion-Pumping Microbial Rhodopsins. *Front. Mol. Biosci.* **2015**, *2*, 52.

(5) Gunaydin, L. A.; Yizhar, O.; Berndt, A.; Sohal, V. S.; Deisseroth, K.; Hegemann, P. Ultrafast Optogenetic Control. *Nat. Neurosci.* **2010**, *13* (3), 387–392.

(6) Oesterhelt, D.; Stoeckenius, W. Rhodopsin-Like Protein From the Purple Membrane of *Halobacterium Halobium*. *Nature New Biol.* **1971**, *233* (39), 149–152.

(7) Birge, R. R. Nature of the Primary Photochemical Events in Rhodopsin and Bacteriorhodopsin. *Biochim. Biophys. Acta* **1990**, *1016* (3), 293–327.

(8) Haupts, U.; Tittor, J.; Oesterhelt, D. Closing in on Bacteriorhodopsin: Progress in Understanding the Molecule. *Annu. Rev. Biophys. Biomol. Struct.* **1999**, *28* (1), 367–399.

(9) Lanyi, J. K. Bacteriorhodopsin. *Annu. Rev. Physiol.* **2004**, *66* (1), 665–688.

(10) Birge, R. R.; Cooper, T. M.; Lawrence, A. F.; Masthay, M. B.; Zhang, C. F.; Zidovetzki, R. Revised Assignment of Energy Storage in the Primary Photochemical Event in Bacteriorhodopsin. *J. Am. Chem. Soc.* **1991**, *113* (11), 4327–4328.

(11) Logunov, S. L.; El-Sayed, M. A. Redetermination of the Quantum Yield of Photoisomerization and Energy Content in the K-Intermediate of Bacteriorhodopsin Photocycle and Its Mutants by the Photoacoustic Technique. *J. Phys. Chem. B* **1997**, *101* (33), 6629–6633.

(12) Govindjee, R.; Balashov, S. P.; Ebrey, T. G. Quantum Efficiency of the Photochemical Cycle of Bacteriorhodopsin. *Biophys. J.* **1990**, *58* (3), 597–608.

(13) Oesterhelt, D.; Hegemann, P.; Tittor, J. The Photocycle of the Chloride Pump Halorhodopsin. II: Quantum Yields and a Kinetic Model. *EMBO J.* **1985**, *4* (9), 2351–2356.

(14) Tittor, J.; Oesterhelt, D. The Quantum Yield of Bacteriorhodopsin. *FEBS Letters* **1990**, *263* (2), 269–273.

(15) Kandori, H.; Sasabe, H. Excited-State Dynamics of a Protonated Schiff Base of All-*Trans* Retinal in Methanol Probed by Femtosecond Fluorescence Measurement. *Chem. Phys. Lett.* **1993**, *216* (1-2), 126–172.

(16) Logunov, S. L.; Song, L.; El-Sayed, M. A. Excited-State Dynamics of a Protonated Retinal Schiff Base in Solution. *J. Phys. Chem.* **1996**, *100* (47), 18586–18591.

(17) Mathies, R. A.; Brito Cruz, C. H.; Pollard, W. T.; Shank, C. V. Direct Observation of the Femtosecond Excited-State *Cis-Trans* Isomerization in Bacteriorhodopsin. *Science* **1988**, *240* (4853), 777–779.

(18) Kandori, H.; Yoshihara, K.; Tomioka, H.; Sasabe, H. Primary Photochemical Events in Halorhodopsin Studied by Subpicosecond Time-Resolved Spectroscopy. *J. Phys. Chem.* **1992**, *96* (14), 6066–6071.

(19) Arlt, T.; Schmidt, S.; Zinth, W.; Haupts, U.; Oesterhelt, D. The Initial Reaction Dynamics of the Light-Driven Chloride Pump Halorhodopsin. *Chem. Phys. Lett.* **1995**, *241* (5-6), 559–565.

(20) Lenz, M. O.; Huber, R.; Schmidt, B.; Gilch, P.; Kalmbach, R.; Engelhard, M.; Wachtveitl, J. First Steps of Retinal Photoisomerization in Proteorhodopsin. *Biophys. J.* **2006**, *91* (1), 255–262.

(21) Wand, A.; Loevsky, B.; Friedman, N.; Sheves, M.; Ruhman, S. Probing Ultrafast Photochemistry of Retinal Proteins in the Near-IR: Bacteriorhodopsin and *Anabaena* Sensory Rhodopsin vs Retinal Protonated Schiff Base in Solution. *J. Phys. Chem. B* **2012**, *117* (16), 4670–4679.

(22) Tahara, S.; Takeuchi, S.; Abe-Yoshizumi, R.; Inoue, K.; Ohtani, H.; Kandori, H.; Tahara, T. Ultrafast Photoreaction Dynamics of a Light-Driven Sodium-Ion-Pumping Retinal Protein from *Krokinobacter eikastus* Revealed by Femtosecond Time-Resolved Absorption Spectroscopy. *J. Phys. Chem. Lett.* **2015**, *6* (22), 4481–4486.

(23) Nuss, M. C.; Zinth, W.; Kaiser, W.; Kölling, E.; Oesterhelt, D. Femtosecond Spectroscopy of the First Events of the Photochemical Cycle in Bacteriorhodopsin. *Chem. Phys. Lett.* **1985**, *117* (1), 1–7.

(24) Polland, H. J.; Franz, M. A.; Zinth, W.; Kaiser, W.; Kölling, E.; Oesterhelt, D. Early Picosecond Events in the Photocycle of Bacteriorhodopsin. *Biophys. J.* **1986**, *49* (3), 651–662.

(25) Huber, R.; Köhler, T.; Lenz, M. O.; Bamberg, E.; Kalmbach, R.; Engelhard, M.; Wachtveitl, J. pH-Dependent Photoisomerization of Retinal in Proteorhodopsin. *Biochemistry* **2005**, *44* (6), 1800–1806.

(26) Marín, M. D. C.; Agathangelou, D.; Orozco-Gonzalez, Y.; Valentini, A.; Kato, Y.; Abe-Yoshizumi, R.; Kandori, H.; Choi, A.; Jung, K.-H.; Haacke, S.; et al. Fluorescence Enhancement of a Microbial Rhodopsin via Electronic Reprogramming. *J. Am. Chem. Soc.* **2019**, *141* (1), 262–271.

(27) Nakamura, T.; Takeuchi, S.; Shibata, M.; Demura, M.; Kandori, H.; Tahara, T. Ultrafast Pump−Probe Study of the Primary Photoreaction Process in *pharaonis* Halorhodopsin: Halide Ion Dependence and Isomerization Dynamics. *J. Phys. Chem. B* **2008**, *112* (40), 12795–12800.

(28) Sudo, Y.; Mizuno, M.; Wei, Z.; Takeuchi, S.; Tahara, T.; Mizutani, Y. The Early Steps in the Photocycle of a Photosensor Protein Sensory Rhodopsin I From *Salinibacter Ruber*. *J. Phys. Chem. B* **2014**, *118* (6), 1510–1518.

(29) Tahara, S.; Takeuchi, S.; Abe-Yoshizumi, R.; Inoue, K.; Ohtani, H.; Kandori, H.; Tahara, T. Origin of the Reactive and Nonreactive Excited States in the Primary Reaction of Rhodopsins: pH Dependence of Femtosecond Absorption of Light-Driven Sodium Ion Pump Rhodopsin KR2. *J. Phys. Chem. B* **2018**, *122* (18), 4784–4792.

(30) Inoue, K.; Ono, H.; Abe-Yoshizumi, R.; Yoshizawa, S.; Ito, H.; Kogure, K.; Kandori, H. A Light-Driven Sodium Ion Pump in Marine Bacteria. *Nat. Commun.* **2013**, *4* (1), 1678.

(31) Kato, H. E.; Inoue, K.; Abe-Yoshizumi, R.; Kato, Y.; Ono, H.; Konno, M.; Hososhima, S.; Ishizuka, T.; Hoque, M. R.; Kunitomo, H.; et al. Structural Basis for Na^+ Transport Mechanism by a Light-Driven Na^+ Pump. *Nature* **2015**, *521* (7550), 48–53.

Chapter 2.

Experimental Methods

2.1 Femtosecond Time-Resolved Absorption Spectroscopy

2.1.1 Principle of Femtosecond Time-Resolved Absorption Spectroscopy

In order to track the excited-state dynamics of the photochemical reaction on the femtosecond-to-picosecond time scale, several femtosecond time-resolved spectroscopic techniques have been developed to date, yet femtosecond time-resolved absorption spectroscopy remains the most common and powerful tool. It captures the electronic absorption spectra of the transients and provides qualitative and quantitative information on these transient species.

Femtosecond time-resolved absorption measurement is performed with so-called pump-probe manner, which is schematically illustrated in Figure 2.1. A monochromatic pump pulse, having a temporal bandwidth shorter than a picosecond, first encounters the sample cell to excite the molecules of interest to their electronic excited states by a vertical Franck-Condon transition and initiates the photoreaction. After a certain delay time Δt, another weak (broadband or monochromatic) probe pulse arrives and measures the transient absorbance of the sample. By variating the time delay Δt between the pump and probe pulses using a computer-controlled optical delay, a series of time-resolved absorption spectra can be obtained and the transient species in the photoreaction is therefore captured.

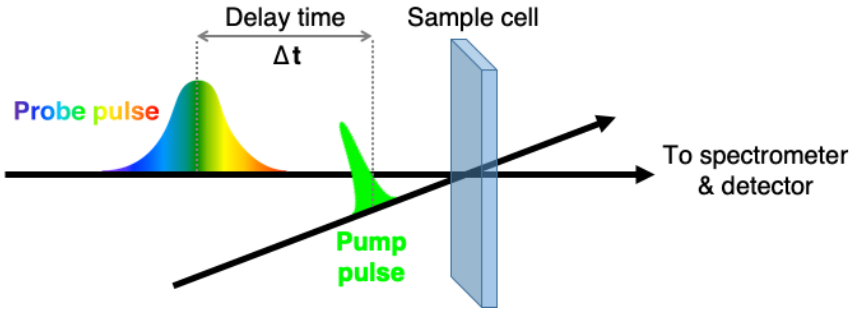

Figure 2.1 Principle scheme of the femtosecond time-resolved absorption experiment.

To emphasize the excited-state signals and the photo-induced species, the time-resolved absorption spectrum is plotted as the difference absorbance $\Delta A(\lambda, \Delta t)$ with and without the presence of the pump pulse:

$$\Delta A(\lambda, \Delta t) = A_{\text{pump on}} - A_{\text{pump off}} = -log \frac{I_{probe}^{\text{pump on}} / I_{ref}^{\text{pump on}}}{I_{probe}^{\text{pump off}} / I_{ref}^{\text{pump off}}}$$

where $I_{probe}^{\text{pump on}}$ and $I_{probe}^{\text{pump off}}$ are the probe intensities at wavelength λ with and without the pump pulse at delay time Δt, respectively. In the actual measurement, a portion of the probe pulse is used as the reference pulse, and their intensities $I_{ref}^{\text{pump on}}$ and $I_{ref}^{\text{pump off}}$ are simultaneously monitored by a detector to eliminate the intensity fluctuation of the probe pulse.

Figure 2.2(a) shows a typical femtosecond time-resolved absorption spectrum at an arbitrary delay time. It contains the transient signals from four different optical processes,[1,2] and their electronic transitions are depicted in Figure 2.2(b):

(1) The first contribution is by the ground-state bleaching (GSB) signal, which corresponds to $S_1 \leftarrow S_0$ transition. When a fraction of the molecules in the ground state are promoted to the excited state by the pump pulse, the probe pulse is therefore less absorbed in the wavelength region of the ground-state absorption, resulting in a negative ΔA signal.

(2) The second contribution to the time-resolved absorption spectrum the stimulated emission (SE) signal related to $S_1 \rightarrow S_0$ transition. The molecules in the excited state can return to their ground state by emission of light, i.e., SE. In general, the spectral profile of the SE signal follows the stationary fluorescence spectrum of the excited molecule, which is Stokes-shifted with respect to the GSB signal. The SE signal increases the probe pulse intensity on the detector, giving rise to a negative ΔA signal.

(3) The third contribution is by the excited-state absorption (ESA) signal. After photoexcitation, optically allowed transition from the excited state to a higher excited state ($S_n \leftarrow S_1$ transition)

may occurs in a certain wavelength region. Such a transition absorbs the probe light, so a positive ΔA signal is observed in the wavelength region of the ESA signal.

(4) The fourth possible contribution to the spectrum is the photoproduct absorption (PA) signal. Upon photoexcitation, the photochemical reaction may take place, producing a newly formed transient or a long-lived molecular state. Absorption from such a newly formed photoproduct state appears as a positive ΔA signal in the time-resolved absorption spectrum.

Because the ESA and SE signals appear only when the excited state is populated, analyzing the temporal change of these signals allow us to understand the excited-state dynamics during the photoreaction.

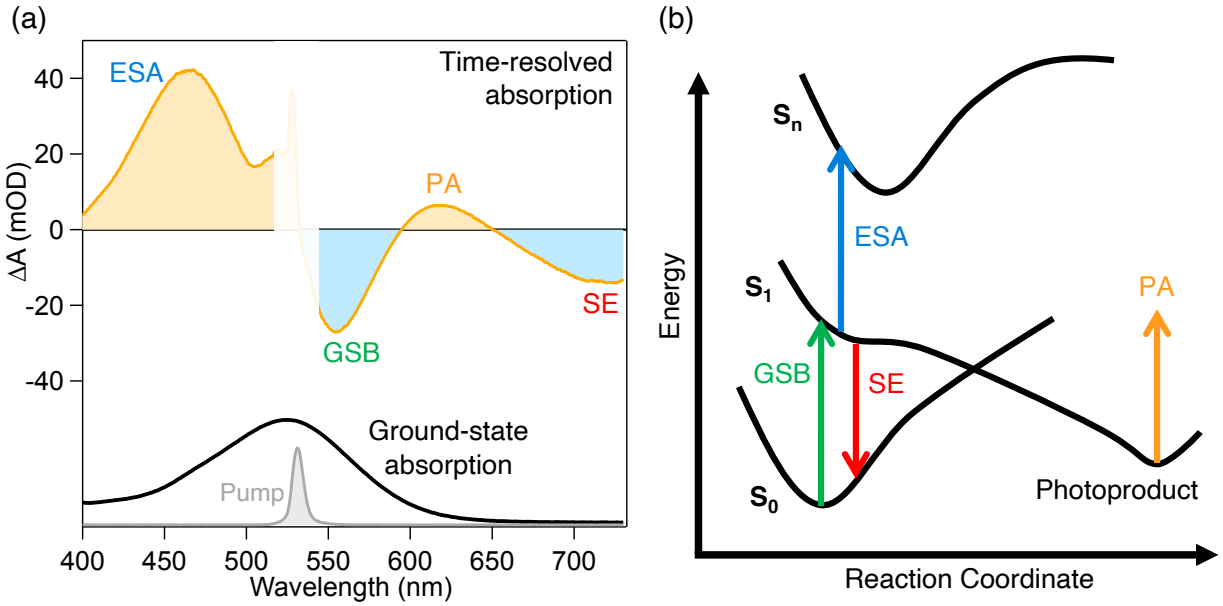

Figure 2.2 (a) Typical femtosecond time-resolved absorption spectrum of the excited molecule at an arbitrary delay time. The ground-state absorption and the pump spectra are shown below for comparison. The white shaded region is masked due to the disturbance of the scattered pump. (b) Electronic transitions of the four transient signals (GSB, ESA, SE and PA) in the time-resolved absorption spectrum in (a). GSB: ground-state bleaching; ESA: excited-state absorption; SE: stimulated emission; PA: photoproduct absorption.

2.1.2 Femtosecond Time-Resolved Absorption Experimental Setup

The schematic of the femtosecond time-resolved absorption spectrometer is depicted in Figure 2.1. A Ti:sapphire regenerative amplifier (800 nm, 1 mJ, 1 kHz, 100 fs, Legend Elite, Coherent) was used as the light source. The output of the amplifier was divided into two portions. The major portion (0.8 mJ) was used for driving an optical parametric amplifier (TOPAS-C, Light Conversion), which is used for generating the pump pulse. The remaining portion of the amplifier output was attenuated and focused into a 3 mm-thick calcium fluoride (CaF_2) plate to generate a white-light continuum.[3] The white-light continuum was split into two, and they were used as the probe and reference pulses. The pump and probe pulses were focused non-collinearly into the sample solution contained in a flow cell. At the sample position, the beam diameters ($1/e^2$) of the pump and probe pulses were ~150 and ~100 μm, respectively. The polarization of the pump pulse was set at the magic angle (54.7˚) with respect to the probe pulse. The sample solution was flowed at the rate sufficient to replace the excited volume between the laser shots. The transmitted probe pulse after the sample as well as the reference pulse was spectrally dispersed by a spectrometer (500is/sm, Chromex), and detected by a CCD camera (PIXIS: 256E, Princeton Instruments). The wavelength-dependent time origin of the chirped white-light probe was corrected by the optical Kerr effect (OKE) signal of the solvent.[4]

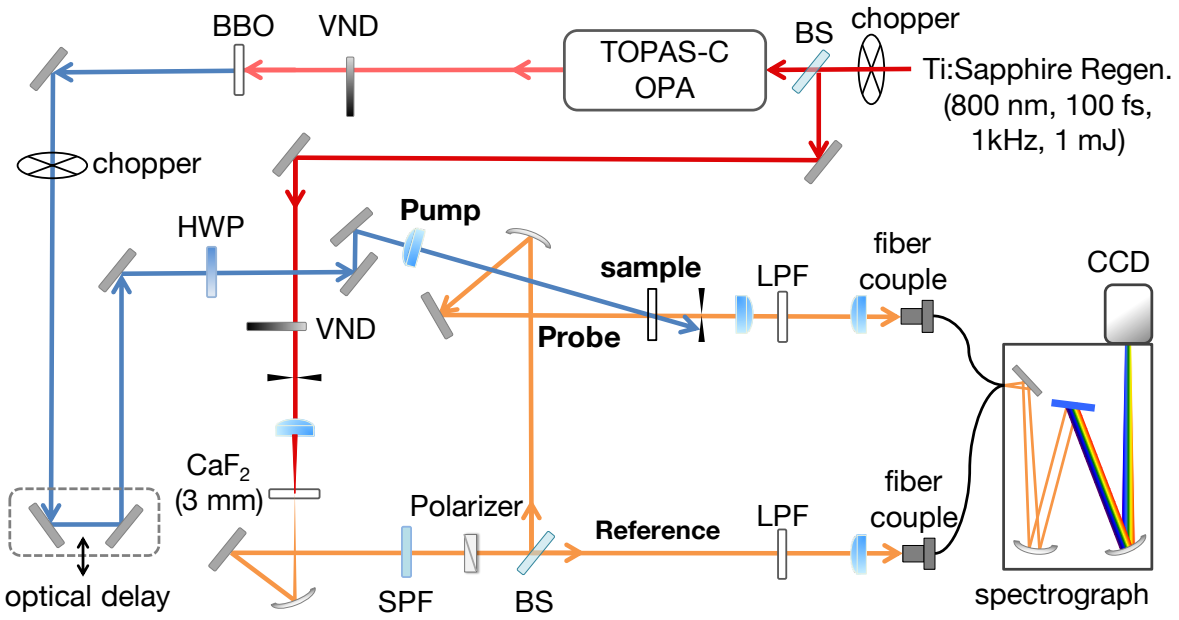

Figure 2.3 Schematic of the femtosecond time-resolved absorption spectrometer. (BS: beam splitter, SPF: short-pass filter, LPF: long-pass filter, HWP: half-wave plate, VND: variable neutral density filter)

2.2 Impulsive Stimulated Raman Spectroscopy

2.2.1 Principle of Impulsive Stimulated Raman Spectroscopy

Stimulated Raman scattering (SRS) is a third-order nonlinear optical process discovered in 1960,[5] which probes the molecular vibrations same as spontaneous Raman scattering. However, unlike spontaneous Raman is an incoherent scattering process, the Raman vibrational motions in SRS are prepared in coherent fashion. The unison molecular vibrations create a coherent polarization in the sample, making the subsequent SRS radiation highly directional and strong.[6] The stronger SRS radiation offers higher signal detection efficiency than spontaneous Raman scattering, enabling observation of considerably weak Raman signals.

Because of the recent advancement of the ultrashort laser pulses, the SRS signals can be measured in time domain, namely impulsive stimulated Raman spectroscopy (ISRS).[7-9] In the ISRS process, an ultrashort Raman pump pulse that is shorter than periods of typical molecular vibrations (10–1000 fs, corresponding to ~33–3333 cm^{-1} vibrations) impulsively excites the Raman-active vibrations of the molecule. The induced vibrational coherence evolves in time, and this time evolution corresponds to the real-time motion of the nuclei of the molecule, which is called the nuclear wavepacket motion. The nuclear wavepacket motion creates the oscillatory changes of the refractive index, which can be measured by another ultrashort probe pulse. By scanning the delay time τ between the Raman pump and probe pulses, the coherently induced nuclear wavepacket motion can be recorded in time domain.

The ISRS experiment can be performed with the pump-probe spectroscopic scheme same as depicted in Figure 2.1, in which both Raman pump and probe pulses have an ultrashort (<10 fs) temporal width. Figure 2.5(a) shows the typical ISRS raw data, containing the population dynamics and the oscillatory component originated from the coherent wavepacket motion. The

population dynamics corresponds to the transiently induced absorption or emission signals produced by the Raman pump pulse (black curve in Figure 2.5(a)). After subtracting the population dynamics from the raw ISRS data, the oscillatory component can be extracted (Figure 2.5(b)). Fourier transformation of the extracted oscillatory component provides the Raman spectrum of the molecule (Figure 2.5(c)). The Raman spectrum obtained with the time-domain ISRS approach has many advantages over the conventional frequency-domain SRS approach: First, ISRS can directly access the low-frequency (<400 cm^{-1}) region, which is difficult to attain by the frequency-domain approach. Secondly, ISRS is free from the nontrivial backgrounds and the interfering line shapes that is often suffered in the frequency-domain measurement.[10-12]

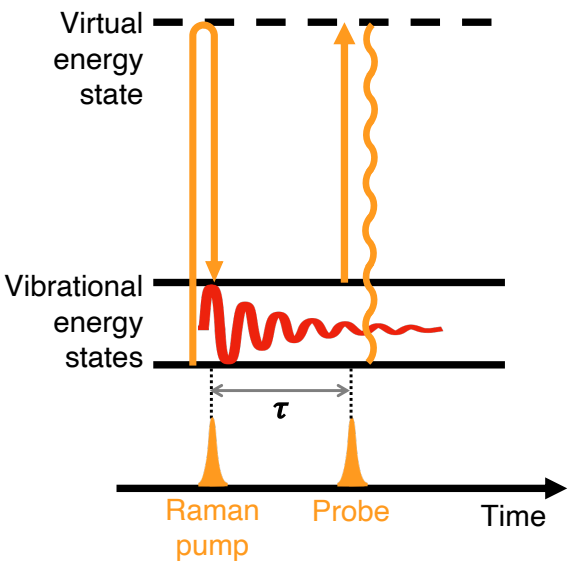

Figure 2.4 Schematic of the optical transitions and the pulse sequence involved in the ISRS experiment.

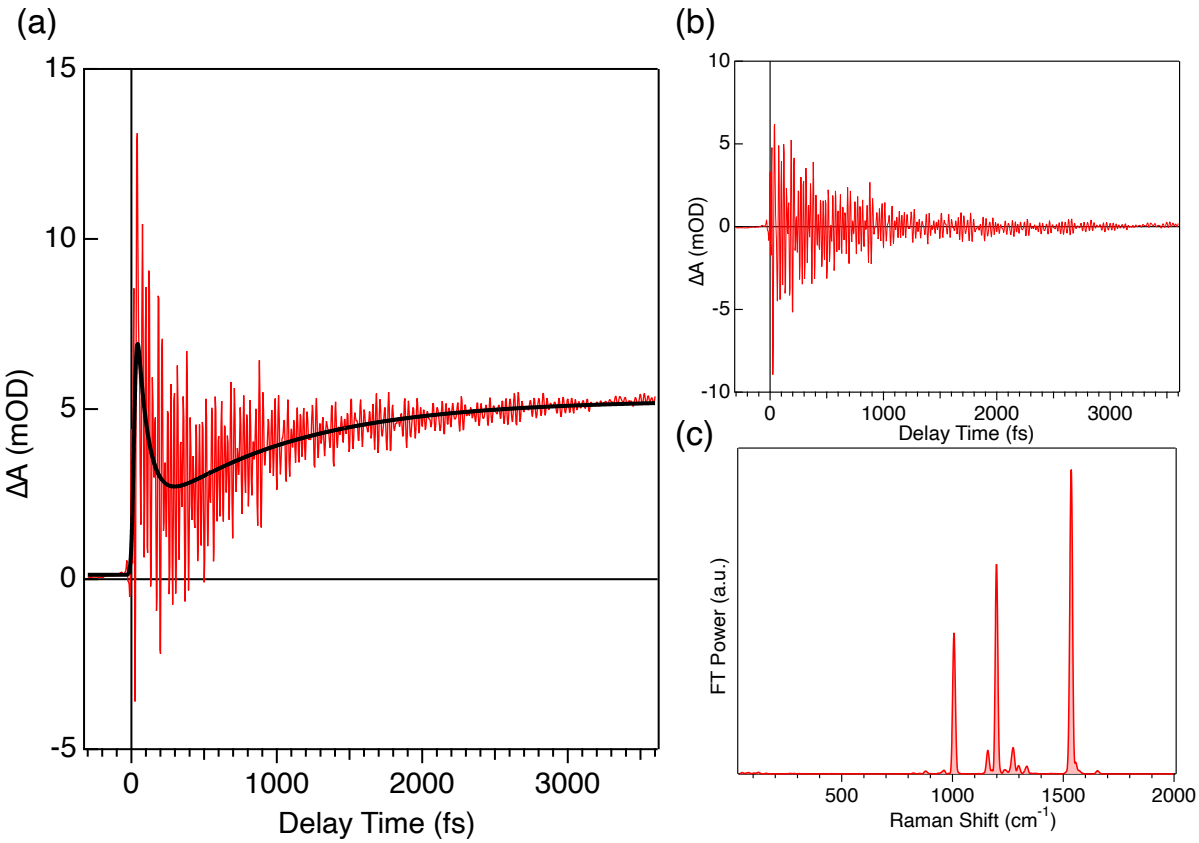

Figure 2.5 (a) Typical pump-probe data detected by a single-channel photodiode in the ISRS experiment. The black curve is the best fit to the data using a sum of exponential functions convoluted with the instrumental response. (b) The oscillatory component of the pump-probe signal, which is coherently induced nuclear wavepacket motion. (c) Fourier-transform power spectrum of the oscillatory component in (b), which represents the Raman spectrum of the molecule.

2.2.2 Impulsive Stimulated Raman Experimental Setup

The schematic of the impulsive stimulated Raman setup is displayed in Figure 2.6. The Ti:sapphire regenerative amplifier (800 nm, 1 mJ, 1 kHz, 100 fs, Legend Elite, Coherent) was used as the light source. The output of the amplifier was used to drive two home-built noncolinear optical parametric amplifiers (NOPAs).[13] The first NOPA (NOPA 1) was used to generate the actinic pump pulse for the time-resolved ISRS measurement, which was not used in the present thesis study. The second NOPA (NOPA 2) was tuned for generating the broad output spectrum. The output of the broad NOPA spectrum was compressed by a pair of fused-silica prisms (45˚ apex angle) and a grating-based 4*f* dispersion compensator equipped with a micro-machined membrane deformable mirror (MMDM) (OKO tech) at the Fourier plane. The compressed pulse was divided into two and used for the Raman pump and probe pulses. A small portion of the probe pulse was picked up for the reference pulse. The Raman pump and probe pulses were focus into the sample solution contained in a flow cell by a concave mirror, having the beam diameters ($1/e^2$) of ~100 and ~90 μm, respectively. The cross-correlation of the Raman pump and probe pulses were characterized by using self-diffraction (SD) or second-harmonic generation (SHG) frequency resolved optical grating (FROG).[14] The intensities of the transmitted probe and reference pulses were detected by the single-channel Si photodiodes (S2281, Hamamatsu Photonics).

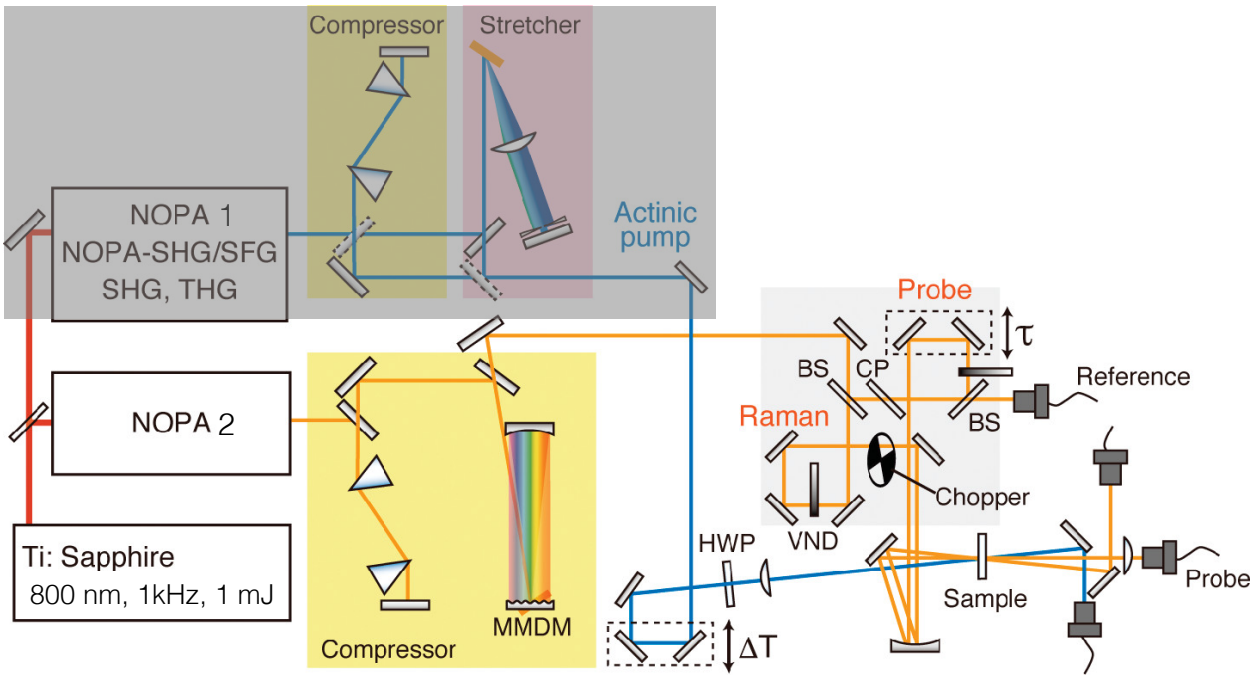

Figure 2.6 Schematic of the impulsive stimulated Raman spectrometer. The optical path in the gray shaded region is not used in the present thesis study. (NOPA: noncollinear optical parametric amplifier; MMDM: micro-machined membrane deformable mirror; HWP: half wave plate; BS: beam splitter; CP: compensation plate; VND: variable neutral density filter.) Reproduced with permission from *Rev. Sci. Instrum.* 2016, 87, 043197. Copyright (2016) AIP Publishing LLC.

References

(1) Berera, R.; van Grondelle, R.; Kennis, J. T. M. Ultrafast Transient Absorption Spectroscopy: Principles and Application to Photosynthetic Systems. *Photosynth Res* **2009**, *101*, 105–118.

(2) Ruckebusch, C.; Sliwa, M.; Pernot, P.; de Juan, A.; Tauler, R. Comprehensive Data Analysis of Femtosecond Transient Absorption Spectra: A Review. *J. Photochem. and Photobiol. C* **2012**, *13* (1), 1–27.

(3) Johnson, P. J. M.; Prokhorenko, V. I.; Miller, R. J. D. Stable UV to IR Supercontinuum Generation in Calcium Fluoride with Conserved Circular Polarization States. *Opt. Express* **2009**, *17* (24), 21488–21496.

(4) Yamaguchi, S.; Hamaguchi, H.-O. Convenient Method of Measuring the Chirp Structure of Femtosecond White-Light Continuum Pulses. *Appl. Spectrosc.* **1995**, *49* (10), 1513–1515.

(5) Maiman, T. H. Stimulated Optical Radiation in Ruby. *Nature* **1960**, *187*, 493–494.

(6) Prince, R. C.; Frontiera, R. R.; Potma, E. O. Stimulated Raman Scattering: From Bulk to Nano. *Chem. Rev.* **2017**, *117* (7), 5070–5094.

(7) Ruhman, S.; Joly, A. G.; Nelson, K. A. Time-Resolved Observations of Coherent Molecular Vibrational Motion and the General Occurrence of Impulsive Stimulated Scattering. *J. Chem. Phys.* **1987**, *86* (11), 6563–6565.

(8) Dhar, L.; Rogers, J. A.; Nelson, K. A. Time-Resolved Vibrational Spectroscopy in the Impulsive Limit. *Chem. Rev.* **1994**, *94* (1), 157–193.

(9) Kuramochi, H.; Takeuchi, S.; Tahara, T. Femtosecond Time-Resolved Impulsive Stimulated Raman Spectroscopy Using Sub-7-Fs Pulses: Apparatus and Applications. *Rev. Sci. Instrum.* **2016**, *87* (4), 043107.

(10) Kukura, P.; McCamant, D. W.; Mathies, R. A. Femtosecond Stimulated Raman Spectroscopy. *Annu. Rev. Phys. Chem.* **2007**, *58* (1), 461–488.

(11) Frontiera, R. R.; Shim, S.; Mathies, R. A. Origin of Negative and Dispersive Features in Anti-Stokes and Resonance Femtosecond Stimulated Raman Spectroscopy. *J. Chem. Phys.* **2008**, *129* (6), 064507.

(12) Weigel, A.; Dobryakov, A.; Klaumünzer, B.; Sajadi, M.; Saalfrank, P.; Ernsting, N. P. Femtosecond Stimulated Raman Spectroscopy of Flavin After Optical Excitation. *J. Phys. Chem. B* **2011**, *115* (13), 3656–3680.

(13) Cerullo, G.; De Silvestri, S. Ultrafast Optical Parametric Amplifiers. *Rev. Sci. Instrum.* **2003**, *74* (1), 1–18.

(14) Trebino, R.; Kane, D. Using Phase Retrieval to Measure the Intensity and Phase of Ultrashort Pulses: Frequency-Resolved Optical Gating. *J. Opt. Soc. Am. A* **1993**, *10* (5), 1101–1111.

Chapter 3.

The Primary Photoreaction in the Proton-Pumping Rhodopsins Studied by Femtosecond Time-Resolved Absorption Spectroscopy

本章については、

５年以内に雑誌等で刊行予定のため、

非公開。

A part of the content in this chapter has been published in the following paper.

“Acid–base equilibrium of the chromophore counterion results in distinct photoisomerization reactivity in the primary event of proteorhodopsin.”

Chang, C.-F.; Kuramochi, H.; Singh, M.; Abe-Yoshizumi, R.; Tsukuda, T.; Kandori, H.; Tahara, T.

Phys. Chem. Chem. Phys. **2019**, 21(46), 25728-25734

Chapter 4.

The Primary Photoreaction in TAT Rhodopsin Studied by Femtosecond Time-Resolved Absorption Spectroscopy

本章については、

５年以内に雑誌等で刊行予定のため、

非公開。

Chapter 5.

Chromophore Structure of Proteorhodopsin and Its pH Dependence Studied by Impulsive Stimulated Raman Spectroscopy

本章については、

５年以内に雑誌等で刊行予定のため、

非公開。

Chapter 6.

Summary and Future Perspective

6.1 Summary

In this thesis, the ultrafast photoisomerization processes in several different microbial rhodopsins were studied by femtosecond time-resolved absorption spectroscopy in order to obtain a coherent view about the primary photoreaction in microbial rhodopsins. In this chapter, the author reviews the observations in Chapter 3 to 5 and describes a generalized primary photoreaction scheme that can be universally applied to all kinds of microbial rhodopsins.

In Chapter 3, the author discussed the primary photoreaction in the proton (H^+)-pumping rhodopsin PR, its D97N mutant and BR which were investigated in a wide range of pH by femtosecond time-resolved absorption spectroscopy. The obtained time-resolved absorption data and quantitative analysis revealed significant pH dependence of the photoisomerization efficiency and excited-state relaxation dynamics in PR and BR. The pH dependence of their excited-state dynamics can be summarized by plotting the relative amplitude of the fast (<1 ps) decay component in the total decay of the stimulated emission (SE) signals against pH, which is shown in Figure 6.1. In both PR and BR, the amplitude of the fast decay component sharply changes at around the pK_a of the protonated Schiff base (PRSB) counterion (7.0–7.9 for Asp97 in PR[1] and 2.05–3.05 for Asp85 in BR,[2] respectively). In particular, the ratio drops from 0.91 to 0.35 in BR when pH is lowered from 4 to 2.5, implying that the fluorescence decay exhibits a clear transition from a single exponential-like decay to a multi-exponential decay. On the other hand, the amplitude of the fast decay component of the point mutant D97N of PR remains the same across the wide range of pH studied, because Asn97 is always neutral. These results unambiguously show that the molecular origin of the multi-exponential decay of the excited state is the acid-base equilibrium of the PRSB counterion in the ground state, as in the case of KR2.[3]

In Chapter 4, the author described the study on the primary photoreaction dynamics of the

recently discovered TAT rhodopsin, which was carried out with femtosecond time-resolved absorption spectroscopy to understand the reason for the absence of the later photocycle intermediate in TAT. The measured time-resolved absorption spectra showed that the K intermediate is barely recognizable, suggesting an extremely low photoisomerization efficiency. Such a low efficiency in the primary reaction prohibits the formation of the subsequent photocycle intermediate, resulting in the absence of the biological function. Moreover, the global fitting analysis showed that the excited-state population decays exclusively with the slow (>1 ps) decay components and no fast (<1 ps) decay component is observed (see Figure 6.1). Interestingly, the analogue residue in TAT rhodopsin with respect to that of the PRSB counterion in PR and BR (Asp97 in PR and Asp85 in BR, respectively) is neutral Thr82.[4] Therefore, the result obtained for TAT rhodopsin is in accordance with that obtained for the H^+-pumping rhodopsins: The retinal photoisomerization is inefficient and the excited state decays predominantly with the slow (>1 ps) decay components when the PRSB counterion is protonated (i.e., neutral). Thus, the primary photoreaction scheme proposed for PR, its D97N mutant and BR having ordinary H^+-pumping function is also applicable to the newly discovered TAT rhodopsin.

In Chapter 5, the author discussed the ground-state structural change of the PRSB chromophore of PR which is associated with the change of the protonation state of counterion Asp97. By measuring the impulsive stimulated Raman spectra with changing the protonation state of Asp97, it was found that the Raman spectra were dramatically changed in the 800–1000 cm^{-1} region, which is assignable to hydrogen-out-of-plane (HOOP) wagging modes of the retinylidene hydrogens.[5] The more numbers the HOOP wagging modes were observed with fully protonated Asp97, which implies that the chromophore has a more distorted structure compared with the one with deprotonated Asp97.[6] The distorted chromophore may not have an optimum geometry for

undergoing the retinal isomerization, which results in the inefficient primary photoisomerization when the counterion Asp97 is protonated.

As summarized in Figure 6.1, this thesis study clarified that the excited-state relaxation dynamics in the primary photoreaction of microbial rhodopsins strongly correlates with the protonation state of their PRSB counterion in the ground state. When the PRSB counterion is deprotonated, the excited state predominantly shows the fast (<1 ps) decay and undergoes photoisomerization efficiently. In contrast, when the PRSB counterion is protonated, the excited state mainly exhibits the slow (>1 ps) decay and preferentially returns to the original ground state instead of undergoing photoisomerization. Although the excited-state relaxation dynamics in different rhodopsins have been explained in terms of the difference in the branching of relaxation pathway on the S_1 potential energy surface without knowing the molecular origin so far,[7-12] the present study unambiguously showed that the difference is, in fact, originated from the difference in the structure in the ground state of microbial rhodopsin, i.e., difference in the protonation state of the PRSB counterion. Therefore, the reaction scheme proposed in Figure 3.18 for PR and BR is highly likely applicable to other microbial rhodopsins in general. The present study provides a new and coherent picture of the primary process in retinal proteins, which takes a big step forward in our fundamental knowledge about the mechanism of light-energy conversion in mother nature.

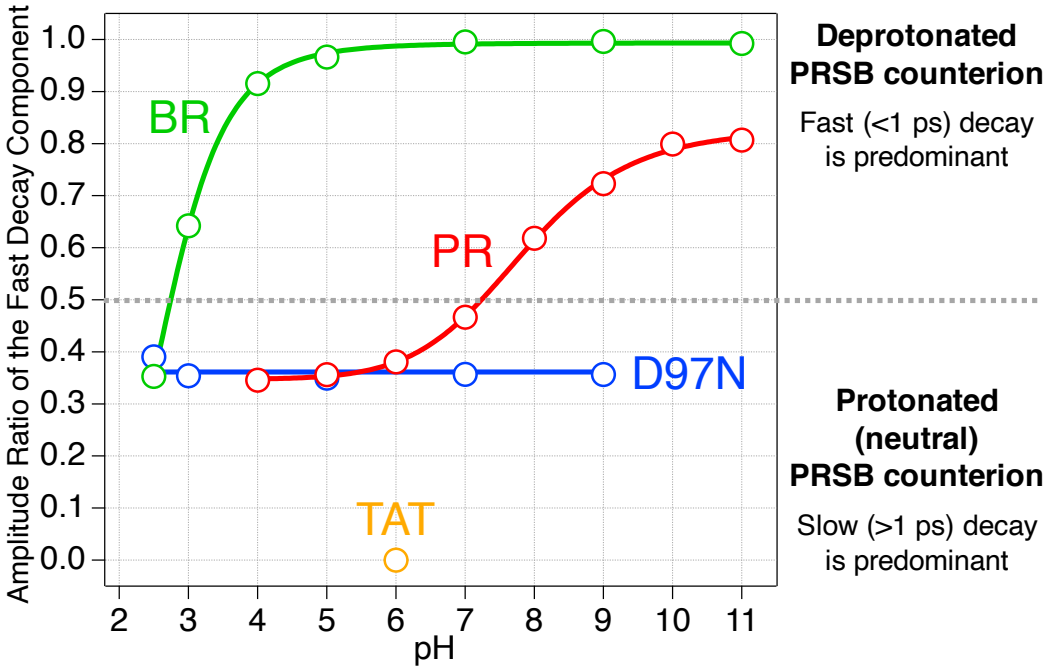

Figure 6.1 Summary of the amplitude ratios of the fast (<1 ps) decay components in the total decays of the SE signals of PR (red circles), its D97N mutant (blue circles), BR (green circles) and TAT rhodopsin (yellow circle). The solid lines are the best fits to the data using the Hill equation for PR and BR and the linear function for the D97N mutant.

6.2 Future Perspective

In this thesis study, femtosecond time-resolved absorption spectroscopy was used to track the ultrafast photoisomerization of retinal proteins. However, one of the drawbacks of time-resolve absorption spectroscopy is spectral overlap of the multiple transient signals due to their broad electronic absorption bandwidths. For example, the photoproduct absorption (PA) signals in PR and BR at acidic pHs suffer from spectral overlap with the ground-state bleaching (GSB) and SE signals, making it difficult to determine the accurate formation time of the photoproduct (the J or K intermediate). Due to the spectral overlap of the PA signal, it is also unclear whether the slow (>1 ps) decay component contributes to formation of the photoproduct or not.

In the attempt to understand the accurate formation dynamics of the photoproduct, time-resolved vibrational spectroscopy is advantageous over electronic spectroscopy due to the narrower bandwidth of the vibrational transition. In particular, time-resolved impulsive stimulated Raman spectroscopy (TR-ISRS) is an ideal methodology for this purpose. TR-ISRS can access femtosecond time resolution while measuring the Raman-active vibrational fingerprints from terahertz to 3000 cm^{-1} simultaneously.[13,14] Recently, the ultrafast structural change in the photoreactions in different protein systems such as green fluorescence protein (GFP)[15] and photoactive yellow protein (PYP)[16] have been successfully probed by TR-ISRS. It would be interesting to capture the structural change in more detail and determine the accurate photoproduct formation dynamics in the primary photoreaction of microbial rhodopsins by TR-ISRS.

Another unanswered question is that the excited-state population does not decay completely with the fast (<1 ps) decay component even if the counterion Asp97 is fully deprotonated in PR. Similarly, even if the counterion Asp97 is fully protonated, the excited-state population exhibits some fast (<1 ps) decay component in PR. Such additional multi-exponential nature of the excited-

state decay may be originated from the branching on the S_1 PES or the additional ground-state heterogeneity. In order to examine whether the additional ground-state heterogeneity plays a role, the double mutant D97N/H75M of PR would be a suitable system for the study using femtosecond time-resolved absorption spectroscopy. As the author proposed in Figure 3.17, the deprotonated Asp97 might selectively forms the weak hydrogen bond with either Thr101 or His75 depending on its orientation, which can create additional heterogeneity. By replacing His75 with the nonpolar methionine, the chromophore environment becomes similar to that of BR.[17] If such an additional heterogeneity plays a role, the D97N/H75M double mutant of PR is expected to only exhibit a single exponential fast (<1 ps) decay of the excited state, as in the case of BR.

References

(1) Sharaabi, Y.; Brumfeld, V.; Sheves, M. Binding of Anions to Proteorhodopsin Affects the Asp97 pK_a. *Biochemistry* **2010**, *49* (21), 4457–4465.

(2) Jonas, R.; Ebrey, T. G. Binding of a Single Divalent Cation Directly Correlates with the Blue-to-Purple Transition in Bacteriorhodopsin. *Proc. Natl. Acad. Sci. U.S.A.* **1991**, *88* (1), 149–153.

(3) Tahara, S.; Takeuchi, S.; Abe-Yoshizumi, R.; Inoue, K.; Ohtani, H.; Kandori, H.; Tahara, T. Origin of the Reactive and Nonreactive Excited States in the Primary Reaction of Rhodopsins: pH Dependence of Femtosecond Absorption of Light-Driven Sodium Ion Pump Rhodopsin KR2. *J. Phys. Chem. B* **2018**, *122* (18), 4784–4792.

(4) Kataoka, C.; Inoue, K.; Katayama, K.; Béjà, O.; Kandori, H. Unique Photochemistry Observed in a New Microbial Rhodopsin. *J. Phys. Chem. Lett.* **2019**, *10* (17), 5117–5121.

(5) Smith, S. O.; Braiman, M. S.; Myers, A. B.; Pardoen, J. A.; Courtin, J. M. L.; Winkel, C.; Lugtenburg, J.; Mathies, R. A. Vibrational Analysis of the All-Trans-Retinal Chromophore in Light-Adapted Bacteriorhodopsin. *J. Am. Chem. Soc.* **1987**, *109* (10), 3108–3125.

(6) Smith, S. O.; Mathies, R. A. Resonance Raman Spectra of the Acidified and Deionized Forms of Bacteriorhodopsin. *Biophys. J.* **1985**, *47* (2), 251–254.

(7) Oesterhelt, D.; Hegemann, P.; Tittor, J. The Photocycle of the Chloride Pump Halorhodopsin. II: Quantum Yields and a Kinetic Model. *EMBO J.* **1985**, *4* (9), 2351–2356.

(8) Govindjee, R.; Balashov, S. P.; Ebrey, T. G. Quantum Efficiency of the Photochemical Cycle of Bacteriorhodopsin. *Biophys. J.* **1990**, *58* (3), 597–608.

(9) Kandori, H.; Yoshihara, K.; Tomioka, H.; Sasabe, H. Primary Photochemical Events in Halorhodopsin Studied by Subpicosecond Time-Resolved Spectroscopy. *J. Phys. Chem.* **1992**, *96* (14), 6066–6071.

(10) Arlt, T.; Schmidt, S.; Zinth, W.; Haupts, U.; Oesterhelt, D. The Initial Reaction Dynamics of the Light-Driven Chloride Pump Halorhodopsin. *Chem. Phys. Lett.* **1995**, *241* (5-6), 559–565.

(11) Nakamura, T.; Takeuchi, S.; Shibata, M.; Demura, M.; Kandori, H.; Tahara, T. Ultrafast Pump−Probe Study of the Primary Photoreaction Process in *pharaonis* Halorhodopsin: Halide Ion Dependence and Isomerization Dynamics. *J. Phys. Chem. B* **2008**, *112* (40), 12795–12800.

(12) Sudo, Y.; Mizuno, M.; Wei, Z.; Takeuchi, S.; Tahara, T.; Mizutani, Y. The Early Steps in the Photocycle of a Photosensor Protein Sensory Rhodopsin I from *Salinibacter* ruber. *J. Phys. Chem. B* **2014**, *118* (6), 1510–1518.

(13) Takeuchi, S.; Ruhman, S.; Tsuneda, T.; Chiba, M.; Taketsugu, T.; Tahara, T. Spectroscopic Tracking of Structural Evolution in Ultrafast Stilbene Photoisomerization. *Science* **2008**, *322* (5904), 1073–1077.

(14) Kuramochi, H.; Takeuchi, S.; Tahara, T. Femtosecond Time-Resolved Impulsive Stimulated Raman Spectroscopy Using Sub-7-Fs Pulses: Apparatus and Applications. *Rev. Sci. Instrum.* **2016**, *87* (4), 043107.

(15) Fujisawa, T.; Fujisawa, T.; Kuramochi, H.; Hosoi, H.; Hosoi, H.; Takeuchi, S.; Tahara, T. Role of Coherent Low-Frequency Motion in Excited-State Proton Transfer of Green Fluorescent Protein Studied by Time-Resolved Impulsive Stimulated Raman Spectroscopy. *J. Am. Chem. Soc.* **2016**, *138* (12), 3942–3945.

(16) Kuramochi, H.; Takeuchi, S.; Yonezawa, K.; Kamikubo, H.; Kataoka, M.; Tahara, T. Probing the Early Stages of Photoreception in Photoactive Yellow Protein with Ultrafast Time-Domain Raman Spectroscopy. *Nat. Chem.* **2017**, *9* (7), 660–666.

(17) Luecke, H.; Schobert, B.; Richter, H. T.; Cartailler, J. P.; Lanyi, J. K. Structure of Bacteriorhodopsin at 1.55 Å Resolution. *J. Mol. Biol.* **1999**, *291* (4), 899–911.

List of Publications and Presentations

Publication related to this thesis

1. "Acid-Base Equilibrium of the Chromophore Counterion Results in Distinct Photoisomerization Reactivity in the Primary Event of Proteorhodopsin."
   C.-F. Chang, H. Kuramochi, M. Singh, R. Abe-Yoshizumi, T. Tsukuda, H. Kandori, T. Tahara, *Phys. Chem. Chem. Phys.* **2019**, 21, 25728-25734.

Publication not related to this thesis

1. "Directly Probing Intermolecular Structural Change of a Core Fragment of β_2-Microglobulin Amyloid Fibrils with Low-Frequency Raman Spectroscopy."
   S. Shigeto, C.-F. Chang, and H. Hiramatsu, *J. Phys. Chem. B* **2017**, 121, 490-496.

Oral presentations

1. "Origin of the Reactive and Nonreactive S_1 States in the Primary Event of Microbial Rhodopsin."
   C.-F. Chang, H. Kuramochi, M. Singh, R. Abe-Yoshizumi, T. Tsukuda, H. Kandori, T. Tahara, 第 13 回分子科学討論会, 1C11, 名古屋, 2019 年 9 月.
2. "Femtosecond Time-resolved Absorption Study on the Origin of the Reactive and Nonreactive Excited States in the Primary Event of Rhodopsins."
   C.-F. Chang, H. Kuramochi, M. Singh, R. Abe-Yoshizumi, T. Tsukuda, H. Kandori, T. Tahara, 日本化学会第 99 春季年会, 3E2-38, 神戸, 2019 年 3 月.

Poster presentation

1. "Ultra-broadband Vis-NIR femtosecond transient absorption spectroscopy of $CH_3NH_3PbI_3$ perovskite thin films."
   C.-F. Chang, H. Kuramochi, S. Takeuchi, T. Tsukuda, E. W.-G. Diau, T. Tahara, 第11回分子科学討論会, 2P037, 仙台, 2017年9月.

Acknowledgements

I would like to first thank Prof. Takashi Nagata and Prof. Tatsuya Tsukuda for providing me with an opportunity to pursue my doctoral study abroad. Their educative consultants helped me to smoothly adapt to the academic system of the University of Tokyo.

The research studies in this thesis were conducted in Molecular Spectroscopy Laboratory (MSL) of RIKEN under supervision of Prof. Tahei Tahara. I would like to express my sincere gratitude to his kind acceptance of me to the fantastic laboratory. His patient guidance and encouragement helped me a lot throughout my PhD study, and the insightful discussions were truly beneficial to my development as an independent researcher. I am also sincerely grateful to Dr. Hikaru Kuramochi of MSL, who carefully mentored me in every details of science, including the femtosecond spectroscopic techniques and the knowledge in molecular science. This thesis study would not be successful without his excellent guidance. Dr. Kunihiko Ishii and Dr. Satoshi Nihonyanagi of MSL are warmly appreciated for their useful discussions and critical comments.

I would like to acknowledge Prof. Hideki Kandori of Nagoya Institute of Technology, who kindly supported the precious rhodopsin samples and gave me fruitful comments. I am also thankful to Prof. Kota Katayama, Dr. Manish Singh, Dr. Rei Abe-Yoshizumi and Mr. Teppei Sugimoto of the Kandori group for their great efforts in making the high-quality rhodopsin samples.

I am indebted to all the members of MSL. Many thanks to the ultrafast spectroscopy team members Dr. Kumar Pardeep, Dr. Tsukasa Takanashi and Dr. Li Liu, who helped me in the daily experiments and shared lots of research ideas. I would also like to give special thanks to the former ultrafast spectroscopy team leader Prof. Satoshi Takeuchi for his mentor in the early stage of my PhD study.

I thank the financial support from the Advanced Leading Graduate Course for Photon Science (ALPS) fellowship of the University of Tokyo. I also thank my ALPS instructor Prof. Takeaki Ozawa for the informative discussions and suggestions on my academic progress.

Last but not the least, I would like to express my deepest appreciation to my parents. It would not be possible to accomplish my PhD research without their continuous financial and spiritual supports.